Neuron, Vol. 40, 581–594, October 30, 2003, Copyright ©2003 by Cell Press

Activity-Dependent mRNA Splicing Controls ER Export and Synaptic Delivery of NMDA Receptors

Yuanyue Mu,[1] Takeshi Otsuka,[1] April C. Horton,[1] Derek B. Scott,[2,3] and Michael D. Ehlers[1,2,3,4,5,*]
[1]Department of Neurobiology
[2]Program in Cell and Molecular Biology
[3]Department of Cell Biology
[4]Department of Pharmacology and Cancer Biology
[5]Neuroproteomics Laboratory
Duke University Medical Center
Box 3209
Durham, North Carolina 27710

Summary

Activity-dependent targeting of NMDA receptors (NMDARs) is a key feature of synapse formation and plasticity. Although mechanisms for rapid trafficking of glutamate receptors have been identified, the molecular events underlying chronic accumulation or loss of synaptic NMDARs have remained unclear. Here we demonstrate that activity controls NMDAR synaptic accumulation by regulating forward trafficking at the endoplasmic reticulum (ER). ER export is accelerated by the alternatively spliced C2′ domain of the NR1 subunit and slowed by the C2 splice cassette. This mRNA splicing event at the C2/C2′ site is activity dependent, with C2′ variants predominating upon activity blockade and C2 variants abundant with increased activity. The switch to C2′ accelerates NMDAR forward trafficking by enhancing recruitment of nascent NMDARs to ER exit sites via binding of a divaline motif within C2′ to COPII coats. These results define a novel pathway underlying activity-dependent targeting of glutamate receptors, providing an unexpected mechanistic link between activity, mRNA splicing, and membrane trafficking during excitatory synapse modification.

Introduction

Experience modifies neural circuitry by use-dependent changes in the number and function of glutamate receptors at excitatory synapses (Carroll and Zukin, 2002; Malinow and Malenka, 2002; Wenthold et al., 2003). Among the glutamate-gated ion channels, N-methyl-D-aspartate (NMDA) receptors (NMDARs) play a central role in synapse formation, synaptic plasticity, and neuropsychiatric disease (Cull-Candy et al., 2001). A principal mechanism controlling NMDAR signaling is accurate regulation of the number of NMDARs present at the synapse (Carroll and Zukin, 2002; Wenthold et al., 2003). Although recent studies have focused on the trafficking of AMPA-type glutamate receptors (AMPARs) (Malinow and Malenka, 2002), dynamic regulation of the number of postsynaptic NMDARs is increasingly recognized as an integral feature of synapse maturation and synaptic plasticity (Carroll and Zukin, 2002; Wenthold et al., 2003). And yet, little is known about the molecular mechanisms for trafficking NMDARs to and from synapses.

Prior to their arrival at the synapse, NMDARs are assembled cotranslationally in the endoplasmic reticulum (ER) from an essential NR1 subunit along with one or more NR2 subunits. The NR1 subunit is encoded by a single gene with three alternatively spliced exons (Zukin and Bennett, 1995). One of them, exon 5, encodes an extracellular N-terminal domain, while exons 21 and 22 encode intracellular C-terminal domains, called C1 and C2, respectively. Exclusion of exon 22 by alternative mRNA splicing introduces a new coding region that encodes an unrelated domain termed C2′ (Zukin and Bennett, 1995). Whereas exon 5 regulates the pharmacological properties of NMDARs (Zukin and Bennett, 1995), mRNA splicing at exons 21 and 22 influences protein interactions and intracellular trafficking whose role in synaptic targeting has been uncertain (Ehlers et al., 1995, 1996, 1998; Okabe et al., 1999; Standley et al., 2000; Scott et al., 2001; Xia et al., 2001).

Synaptic targeting of NMDARs is regulated by activity. For example, in young hippocampal slice cultures, synaptic delivery of NR2A-containing NMDARs requires receptor activation (Barria and Malinow, 2002). In adult hippocampal slice, long-term potentiation (LTP) at CA1 synapses promotes the rapid surface expression of NMDARs and increases NMDAR currents (Grosshans et al., 2002). On the other hand, certain forms of long-term depression (LTD) are accompanied by a rapid decrease in synaptic NMDARs (Heynen et al., 2000). Over much longer time scales of several days, blockade of neuronal activity increases synaptic accumulation of NMDARs and increases the amplitude of NMDAR-mediated miniature excitatory postsynaptic currents (mEPSCs) (Rao and Craig, 1997; Liao et al., 1999; Watt et al., 2000; Crump et al., 2001). Conversely, chronically elevated activity decreases the number of synaptic NMDARs and the size of NMDAR-mediated currents (Rao and Craig, 1997; Liao et al., 1999; Watt et al., 2000; Crump et al., 2001). By reciprocally regulating the number of synaptic receptors, prolonged changes in neuronal activity scale NMDAR-mediated currents proportionally with AMPAR-mediated currents (Watt et al., 2000), providing a cellular mechanism for synaptic homeostasis and a likely basis for metaplasticity—long-term alteration in the ability of a synapse to undergo subsequent potentiation or depression (Abraham and Bear, 1996; Turrigiano and Nelson, 2000).

Although it was one of the very first examples of regulated glutamate receptor trafficking (Rao and Craig, 1997), the molecular and cellular mechanisms underlying long-term activity-dependent synaptic targeting of NMDARs remain poorly understood. Blockade-induced accumulation of synaptic NMDARs is accompanied by an increase in receptor surface expression (Crump et al., 2001), suggesting activity-dependent delivery to the plasma membrane. Moreover, in some cases, experience-dependent NMDAR targeting requires protein synthesis (Quinlan et al., 1999), suggesting regulation at the level of transcription, translation, or mRNA processing. NMDAR

*Correspondence: ehlers@neuro.duke.edu

subunits themselves contain molecular determinants for endocytosis (Roche et al., 2001), synapse association (Barria and Malinow, 2002), scaffold interactions (Wenthold et al., 2003), kinase-induced insertion (Lan et al., 2001; Scott et al., 2001), and surface expression (Okabe et al., 1999; Standley et al., 2000; Scott et al., 2001; Xia et al., 2001), whose relative contributions to synaptic targeting remain unclear. The recent findings that C-terminal domains of the NR1 subunit regulate NMDAR surface expression (Okabe et al., 1999), ER-to-Golgi secretory trafficking (Standley et al., 2000; Scott et al., 2001; Xia et al., 2001), and LTP-dependent surface delivery (Grosshans et al., 2002) point to the possibility for activity-regulated forward trafficking of NMDARs through the secretory pathway. Notably, export from the ER is the rate-limiting step for nearly all membrane proteins to reach the cell surface (Lodish, 1988), and such export is mediated by COPII coats that bud vesicles from the ER for transport to the Golgi (Barlowe, 2002). Yet, little is known about how neuronal activity impinges on the biogenesis and forward trafficking of any neurotransmitter receptor or ion channel.

In this study, we have investigated the effect of activity on forward trafficking of NMDARs through the early secretory pathway and the regulation of such trafficking by mRNA splicing. Using a combination of biochemical, immunocytochemical, and electrophysiological approaches, we demonstrate that newly synthesized NMDARs undergo accelerated transport between the ER and the plasma membrane in the absence of synaptic activity. This hastened export from the ER arises due to altered splicing of NR1 mRNA at exon 22 and incorporation of an export signal that recruits nascent NMDARs to COPII-coated vesicles budding from the ER. These results identify activity-dependent mRNA splicing and ER export as a novel mechanism for bidirectional regulation of NMDAR targeting to the synapse, revealing a potential mechanism for synaptic homeostasis and metaplasticity.

Results

Activity Regulates NR1 mRNA Splicing at the C2/C2′ Site

C-terminal splice variants of NR1 are differentially expressed at the cell surface (Okabe et al., 1999). To test whether activity-dependent NMDAR targeting involves NR1 C-terminal domains, we first examined the influence of neuronal activity on NR1 mRNA splicing (Figure 1A). Expression of C2- and C2′-containing NR1 subunits from cultured cortical neurons (DIV 12–14) was measured following prolonged increases or decreases in activity using splice variant-specific antibodies. Neuronal activity was decreased by blocking action potentials using the Na^+ channel blocker tetrodotoxin (TTX, 2 μM) and increased by blocking inhibitory synaptic inputs with the $GABA_A$ receptor antagonist bicuculline (Bicuc, 40 μM). Upon chronic activity blockade (TTX, 2 μM, 48 hr) or selective antagonism of NMDARs (D-AP5, 100 μM, 7 days), conditions that result in synaptic accumulation of NMDARs (Rao and Craig, 1997; Liao et al., 1999; Crump et al., 2001), the expression of C2′-containing NR1 increased approximately 2-fold (percent relative to control: TTX, 167% ± 9%; AP5, 224% ± 10%; Figures 1B and 1C), whereas C2-containing NR1 decreased (TTX, 59% ± 11%; AP5, 44% ± 7%; Figures 1B and 1C). Conversely, increasing neuronal activity (Bicuc, 40 μM, 48 hr) caused an inverse change in NR1 splice variants, namely an increase in expression of C2-containing NR1 subunits (165% ± 15%) and a decrease in C2′-containing NR1 (61% ± 6%) (Figures 1B and 1C). NMDAR blockade did not itself affect firing frequency in these cultures (control, 0.47 ± 0.08 Hz, n = 11; AP5, 0.43 ± 0.11 Hz, n = 7), indicating that activation of NMDARs is required for the activity-induced changes in NR1 splice variants. Importantly, these reciprocal changes in NR1 splice variant expression occurred without changes in the total amount of NR1 protein (NR1-pan, percent relative to control: TTX, 101% ± 5%; AP5, 112% ± 7%; bicuculline, 97% ± 2%; Figures 1B and 1C). Thus, activity regulates isoform composition but not overall expression of NR1.

To determine whether activity regulates NR1 splice variants at the mRNA level, we performed RNase protection assays using pan-NR1 and C2′-specific probes (Figure 1A) to quantitatively measure NR1 mRNA isolated from cortical neurons after chronic manipulations of activity. Consistent with our results above (Figures 1B and 1C), prolonged activity blockade increased C2′-containing NR1 mRNA (percent relative to control: TTX, 208% ± 19%; and AP5, 189% ± 3%; Figures 1D and 1E). On the other hand, C2′-containing NR1 mRNA was reduced with increased activity (Bicuc, 79% ± 5%, Figures 1D and 1E). This activity-dependent regulation of NR1 mRNA splicing was reversible upon drug washout (Figure 1E) and, as with total NR1 protein (Figure 1C), total NR1 mRNA was unaffected by activity (Figure 1D), indicating no net effect on NR1 gene expression. Since the expression of C2- or C2′-containing NR1 splice variants is determined by inclusion or exclusion of a single exon (Figure 1A), these findings provide direct evidence that splicing at exon 22 of the NR1 pre-mRNA is determined by the level of neuronal activity.

Bidirectional Accumulation of NR1 Splice Variants in the Postsynaptic Density

To test whether activity-dependent NR1 mRNA splicing resulted in corresponding changes in synaptic NMDARs, postsynaptic density (PSD) fractions were isolated from cultured cortical neurons after 48 hr of activity blockade (2 μM TTX) or enhanced excitatory activity (40 μM bicuculline), and the abundance of NR1 splice variants was measured using domain-specific antibodies (Figure 2A). Consistent with previous results (Rao and Craig, 1997; Liao et al., 1999; Watt et al., 2000; Crump et al., 2001; Ehlers, 2003), prolonged activity blockade caused an accumulation of NMDARs in the PSD (NR1-pan, TTX, 181% ± 18% relative to control, Figure 2B). Interestingly, this synaptic accumulation was accompanied by a quantitatively similar accumulation of C2′-containing NR1 subunits in the PSD (TTX, 217% ± 20%, Figures 2A and 2B). Likewise, in PSD fractions from active cultures, NMDARs were decreased in abundance (NR1-pan, Bicuc, 65% ± 19% relative to control) and this decrease was mirrored by a reduction of C2′-containing NR1 subunits (Bicuc, 16% ± 13%, Figures 2A and 2B). In contrast, C2-containing NR1 splice variants had a precisely opposite pattern of synaptic accumulation, exhibiting decreased PSD levels upon activity blockade (TTX,

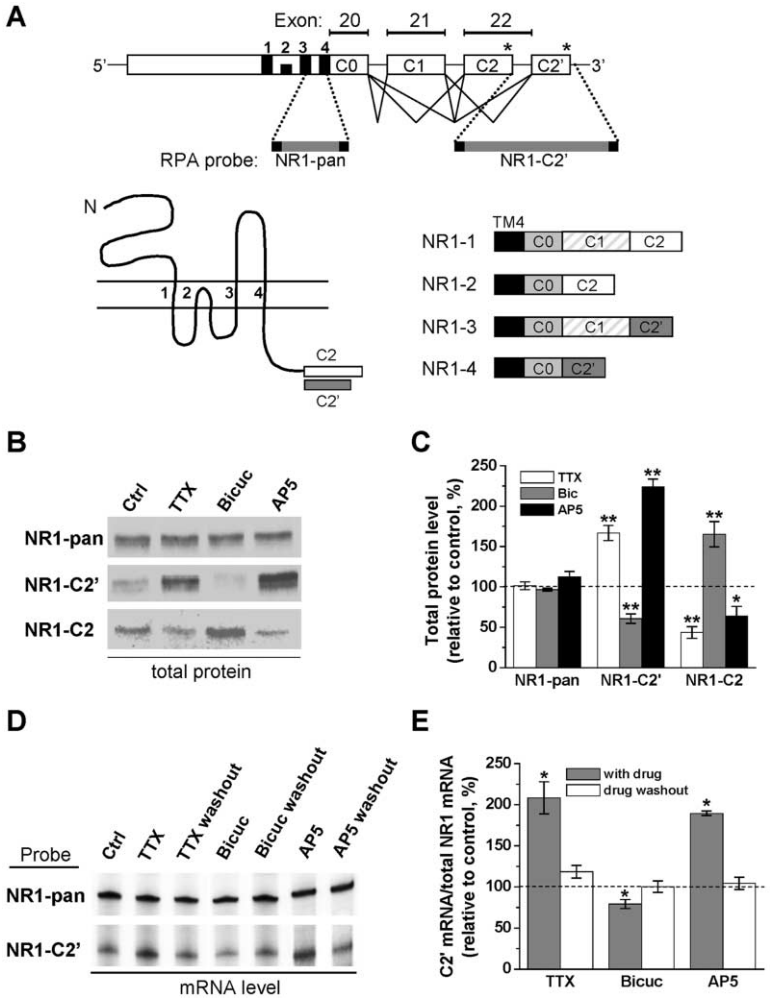

Figure 1. Activity Regulates NR1 mRNA Splicing at Exon 22

(A) Top: Partial diagram of the NR1 gene showing the intron/exon structure of C-terminal splice variants. Exon 22 encodes the C2 C-terminal domain of NR1. Exclusion of exon 22 produces an alternate C-terminal amino acid-encoding sequence termed C2′. Asterisks indicate stop codons in C2 and C2′ domains. Amplified sequences used as probes for RNase protection assays are shown. Dark bars and numbers indicate transmembrane domains. Bottom: Schematic diagram of the NR1 subunit and its C-terminal splice variants. The full-length NR1 polypeptide is shown on the left. The intracellular C termini are shown on the right. Note that all NR1 subunits contain either C2 or C2′.

(B) Activity blockade increases C2′-containing NR1 subunits and decreases C2-containing NR1 subunits. Immunoblot analysis was performed on total protein homogenates from cultured cortical neurons (DIV 12–14). Prior to analysis, cortical neurons were incubated with TTX (2 μM, 2 days), AP5 (100 μM D-AP5, 7 days), or bicuculline (Bicuc, 40 μM, 2 days). Domain-specific antibodies were used to measure the expression of total NR1 (NR1-pan), C2-containing NR1 subunits (NR1-C2), and C2′-containing NR1 subunits (NR1-C2′).

(C) NR1 splice variant protein levels in cortical neurons incubated in TTX, bicuculline, or AP5 as in (B) were quantified by phosphorimager analysis and normalized to control neurons. Plotted data represent means ± SEM from four separate experiments. *$p < 0.01$, **$p < 0.001$ relative to control, t test.

(D) Activity reversibly regulates NR1 splice variants at the mRNA level. RNase protection assays were performed on total RNA isolated from control, TTX-, bicuculline-, or AP5-treated cortical neurons as in (B) before or after a subsequent 2 day period of drug washout. Total NR1 (NR1-pan) and exon 22-excluded (C2′-containing, NR1-C2′) NR1 transcripts were simultaneously detected using specific probes as indicated in (A).

(E) Quantitative analysis of NR1 mRNAs. The plotted data represent the ratio of exon 22-lacking (C2′-containing) NR1 mRNA to total NR1 mRNA in drug-treated neurons relative to control neurons (means ± SEM from four separate experiments, *$p < 0.05$ relative to control, t test).

24% ± 18% relative to control) and increased PSD levels with elevated activity (Bicuc, 197% ± 10%, Figures 2A and 2B). Notably, addition of AP5 (100 μM) and CNQX (10 μM), antagonists of NMDARs and AMPARs, respectively, mimicked the effect of TTX even in the presence of bicuculline (Figures 2A and 2B), indicating a requirement for postsynaptic glutamate receptor activation. Moreover, much like the slow kinetics of activity-dependent synaptic NMDAR accumulation (Rao and Craig, 1997; Liao et al., 1999; Watt et al., 2000; Crump et al., 2001; Ehlers, 2003), the bidirectional change in synaptic NR1 splice variants occurred slowly and reversed completely upon drug washout (Figures 2C and 2D). These experiments show that activity-dependent synaptic targeting of NMDARs is accompanied by selective accumulation of C2′-containing NR1 splice variants in the PSD.

The C2′ Domain Accelerates and the C2 Domain Slows Forward Trafficking

The marked synaptic accumulation of C2′-containing NMDARs upon activity blockade (Figure 2) led us to investigate whether the C2′ and C2 domains of NR1 differentially regulate NMDAR forward trafficking. In initial experiments, the C2 or C2′ domain of NR1 was fused to the intracellular C terminus of Tac, a type I transmembrane protein that has been widely used to study membrane protein trafficking (Figure 3A; Standley et al., 2000; Roche et al., 2001; Scott et al., 2001), and these recombinant fusions were expressed in COS-7 cells. At steady state, Tac is present as both a low molecular mass immature species sensitive to endoglycosidase H (endo H) and as a higher molecular mass mature species resistant to endo H that has traversed the medial Golgi (Figure 3A; Standley et al., 2000; Roche et al., 2001; Scott et al., 2001). Insertion of the C2′ domain at the Tac C terminus increased the endo H-resistant fraction at steady state (82% ± 1%) compared to Tac alone (56% ± 2%, Figures 3A and 3B). Conversely, insertion of C2 resulted in a decrease in the endo H-resistant fraction (14% ± 2%, Figures 3A and 3B). These steady-state results suggested that the C2′ domain facilitates, whereas the C2 domain hinders, maturation of Tac fusion proteins between the ER and Golgi.

To directly measure the kinetics of receptor trafficking through the ER and Golgi, newly synthesized Tac fusions

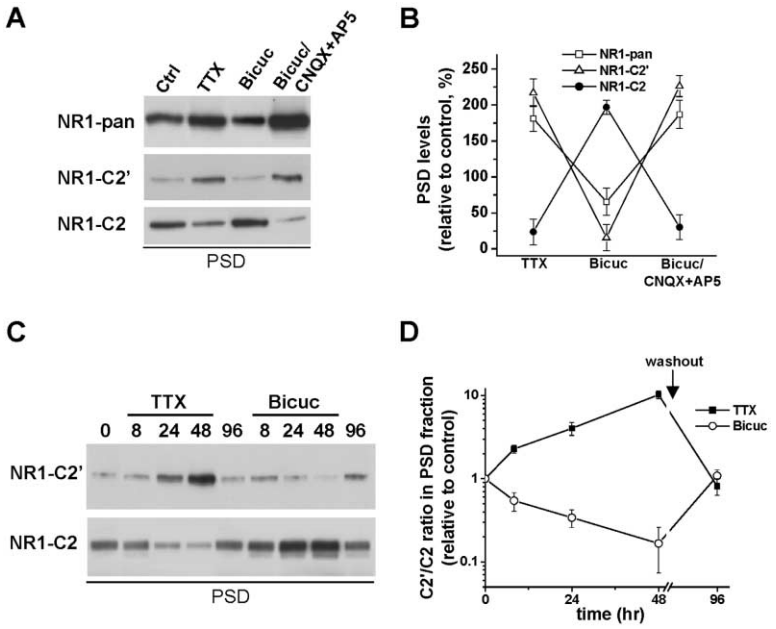

Figure 2. Activity-Dependent Accumulation of NR1 Splice Variants in the Postsynaptic Density

(A) Immunoblot analysis of NR1 splice variants in postsynaptic density (PSD) fractions isolated from control (Ctrl), TTX-, bicuculline (Bicuc)-, or Bicuc plus D-AP5 and CNQX-treated cortical neurons. PSD fractions were resolved by SDS-PAGE and probed for total NR1 (NR1-pan) or for NR1 splice variants containing C2′ (NR1-C2′) or C2 (NR1-C2) domains.

(B) Quantitative analysis of total NR1 (NR1-pan) and NR1 exon 22 splice variants (C2/C2′) in the PSD. Data represent means ± SEM of PSD levels relative to control (n = 4).

(C) Time course and reversibility of NR1 splice variant accumulation or loss in the PSD. Cortical neurons were incubated for various times (numbers in hours) with TTX or bicuculline (Bicuc), or with subsequent 48 hr drug washout (96 hr time points), prior to PSD isolation and immunoblot analysis for NR1-C2′ or NR1-C2.

(D) Activity causes a slow, bidirectional, and reversible switch in synaptic NR1 splice variants. Data represent means ± SEM of C2′/C2 ratios in PSD fractions isolated from TTX- or bicuculline-treated cortical neurons relative to untreated controls (n = 4).

were ^{35}S-labeled and their endo H sensitivity was monitored over time. Tac itself exhibited relatively rapid acquisition of endo H resistance, with 46% ± 1% and 61% ± 2% achieving endo H resistance after 60 min and 120 min, respectively (Figures 3C and 3D). Insertion of the NR1 C2 domain caused a marked slowing of forward trafficking, with only 7% ± 1% and 15% ± 1% of Tac-C2 becoming endo H resistant after 60 min and 120 min chase, respectively (Figures 3C and 3D). On the other hand, appending the C2′ domain to Tac dramatically accelerated the rate of Tac maturation (70% ± 2% and 78% ± 1% mature species after 60 min and 120 min chase, respectively; Figures 3C and 3D), indicating that C2′ and C2 domains serve as positive and negative signals for forward trafficking, respectively.

In order to compare the forward trafficking rates of endogenous C2- and C2′-containing NMDARs, we metabolically labeled newly synthesized receptors in cortical neuron cultures and then measured the time-dependent appearance of labeled receptors at the cell surface by examining their proteolytic sensitivity to extracellularly applied chymotrypsin (Crump et al., 2001; Grosshans et al., 2002), followed by immunoprecipitation with C2- or C2′-specific antibodies. The fraction of remaining intracellular NR1 that contained C2′ was quantified from the relationship ($C2'_{int}/C2_{int} + C2'_{int}$) (Figure 3E). Based on this calculation, if the forward trafficking rate of C2- and C2′-containing NMDARs were equal, the fraction of intracellular NR1 containing C2′ should remain constant over the complete chase period. However, we observed a marked decrease in the $C2'_{int}/C2_{int} + C2'_{int}$ ratio over a 4 hr chase, indicating more rapid acquisition of chymotrypsin sensitivity (and thus more rapid surface delivery) of C2′-containing NMDARs (Figure 3F). Importantly, NR1-C2 and NR1-C2′ display no difference in turnover rates (Huh and Wenthold, 1999), indicating that the differential loss of radiolabel is due to a difference in the kinetics of surface delivery of the two NR1 isoforms. These data provide strong evidence for opposing effects of C2 and C2′ domains on the kinetics of forward trafficking and indicate that C2′ facilitates surface expression of NMDARs by accelerating transport between the ER and Golgi.

The C2′ Domain of NR1 Contains a Novel ER Export Signal

To identify the molecular signal within C2′ that enhances ER export, we performed deletion analysis of the C2′ domain. We concentrated on terminal residues implicated in receptor surface expression (Standley et al., 2000; Scott et al., 2001). Removal of the last three amino acids of C2′ (TVV) dramatically decreased the steady-state abundance of mature endo H-resistant Tac-C2′ (Tac-C2′, 82% ± 1%; Tac-C2′ΔTVV, 37% ± 2%; Figures 4A and 4B), indicating an impairment in forward trafficking. Indeed, monitoring of the kinetics of endo H resistance revealed a marked slowing of Tac-C2′ maturation when the terminal TVV motif was deleted (Figures 4C and 4D), establishing the TVV divaline motif of C2′ as a bona fide ER export signal (Barlowe, 2002). Interestingly, Tac-C2′ΔTVV displayed maturation kinetics similar to Tac alone (endo H-resistant fraction: Tac, 46% ± 1% at 60 min and 61% ± 2% at 120 min; Tac-C2′ΔTVV, 44% ± 1% at 60 min and 60% ± 3% at 120 min; compare Figures 3D and 4D), indicating that the enhancement of forward trafficking by C2′ was largely, if not exclusively, due to the TVV motif.

To test whether the divaline-based ER export motif of C2′ regulates surface expression of NMDARs, we coexpressed NR1 and NR2B subunits in COS-7 cells and

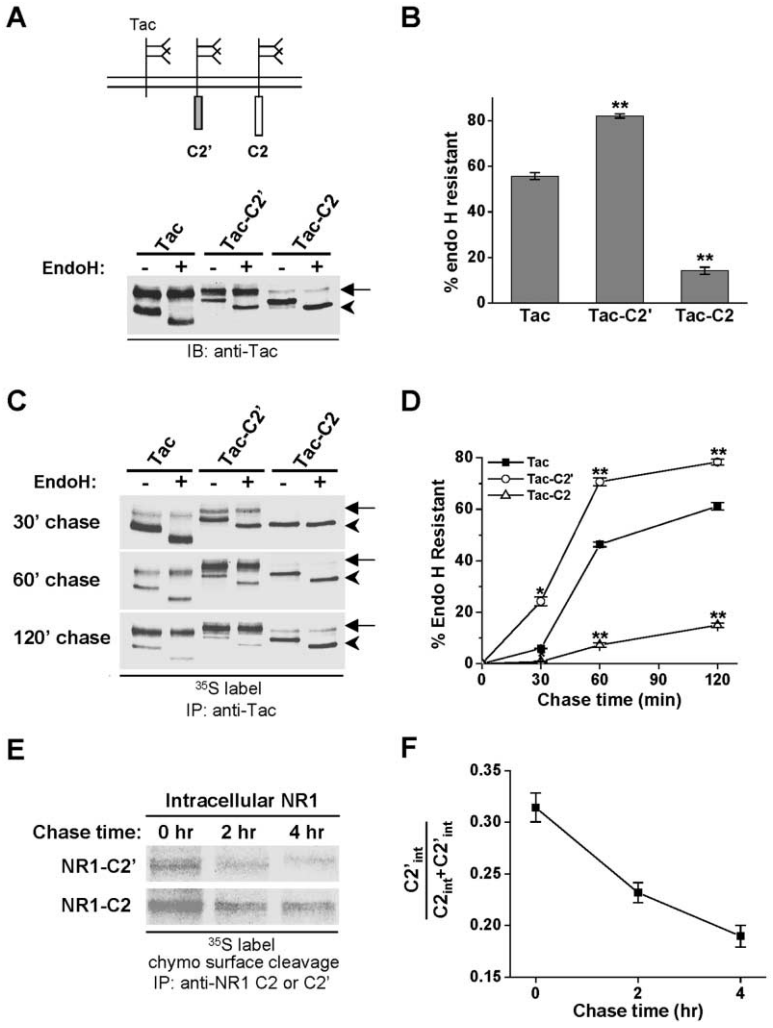

Figure 3. ER-to-Golgi Forward Trafficking Is Enhanced by C2′ and Slowed by C2

(A) C2′ increased while C2 decreased the steady-state levels of mature Tac fusion protein. Endo H sensitivity was measured by deglycosylation of COS-7 cell lysates expressing Tac, Tac-C2′, or Tac-C2 prior to immunoblot analysis. Diagrams of Tac-NR1 receptors are shown (top). The arrow designates mature endo H-resistant Tac species (bottom). The arrowhead indicates immature forms of Tac that are endo H sensitive and thus have not reached the medial Golgi.

(B) Quantification of the percent endo H-resistant Tac species from (A) indicates inverse effects of C2′ and C2 domains on steady-state levels of mature receptor. Plotted data represent means ± SEM from three separate experiments, $^{**}p < 0.001$ relative to Tac alone, t test.

(C) The C2′ domain promotes whereas the C2 domain slows ER export. ER-to-Golgi transport of newly synthesized Tac receptors was monitored by ^{35}S-pulse-chase followed by endo H deglycosylation of labeled Tac immunoprecipitates and autoradiography. Arrow and arrowhead as in (A).

(D) The rate of ER-to-Golgi transport is increased by C2′ and decreased by C2. Plotted data represent means ± SEM of the percent endo H-resistant Tac receptor from (C) at various times of chase ($n = 3$). $^{**}p < 0.001$, $^{*}p < 0.05$ relative to Tac alone, t test.

(E) Surface delivery kinetics of endogenous NR1 splice variants in neurons. Cortical neurons (DIV 12) were labeled with ^{35}S-methionine/cysteine and chased in unlabeled media for the indicated times, and surface proteins were digested with chymotrypsin prior to solubilization and immunoprecipitation for NR1-C2 or NR1-C2′. Remaining intracellular C2- and C2′-containing NMDARs were visualized by autoradiography. Loss of label indicates progressive appearance of NMDARs at the cell surface where they become accessible to chymotrypsin.

(F) Endogenous C2′-containing NMDARs reach the neuronal cell surface more rapidly than C2-containing NMDARs. Plotted data represent means ± SEM of the fraction of remaining intracellular NR1 subunits that contain C2′ ($C2'_{int}/C2_{int} + C2'_{int}$). The decreasing $C2'_{int}/C2_{int} + C2'_{int}$ ratio over time indicates more rapid surface delivery for C2′-containing receptors.

assayed plasma membrane levels by surface biotinylation (Figure 4E). Deletion of the TVV ER export motif caused a significant reduction in surface-expressed NR1/NR2B heteromers (NR1-4/NR2B, 52.9% ± 0.4% at the surface; NR1-4ΔTVV/NR2B, 35.5% ± 0.7%; Figure 4F), consistent with reduced ER export. To determine whether the ER export motif of C2′ likewise regulated NR1 surface expression in neurons, full-length GFP-tagged NR1-4 was expressed in hippocampal neurons and surface receptors were labeled with anti-GFP antibody. Immunofluorescent microscopy revealed that GFP-NR1-4 was robustly expressed at the neuronal cell surface, appearing in puncta throughout the soma and dendrites (Figure 4G), where it localized to glutamatergic synapses (data not shown). A qualitatively similar pattern was observed for GFP-NR1-4ΔTVV (Figure 4H). However, the intensity of surface GFP-NR1-4ΔTVV puncta was notably less than that for wild-type NR1-4 (Figures 4G and 4H). Indeed, quantitative fluorescence measurements revealed a significant decrease in the ratio of surface to total NR1 when the TVV ER export motif was deleted (surface/total ratios: 0.77 ± 0.06, GFP-NR1-4; 0.51 ± 0.10, GFP-NR1-4ΔTVV; Figure 4I). These results expand previous work (Okabe et al., 1999; Standley et al., 2000; Scott et al., 2001; Xia et al., 2001) by showing that the C2′ domain contains an intrinsic ER export motif that accelerates forward trafficking of NR1 and thereby enhances the steady-state surface expression of NMDARs.

The Divaline Motif of NR1-C2′ Binds COPII and Recruits Receptors to ER Exit Sites

ER export requires recruitment of membrane proteins to ER exit sites, where COPII coats bud off vesicles destined for the Golgi (Barlowe, 2002). To test whether the C2′ domain actively recruits nascent receptors to ER exit sites, we took advantage of a temperature-sensitive mutant of the vesicular stomatitis virus glycoprotein (VSVG-ts045) tagged with spectral variants of green fluorescent protein (VSVG-YFP) (Lippincott-Schwartz et al., 2000) and selective temperature block of ER exit (Mezzacasa and Helenius, 2002). At the nonpermissive temperature (39.5°C), VSVG-YFP is misfolded and re-

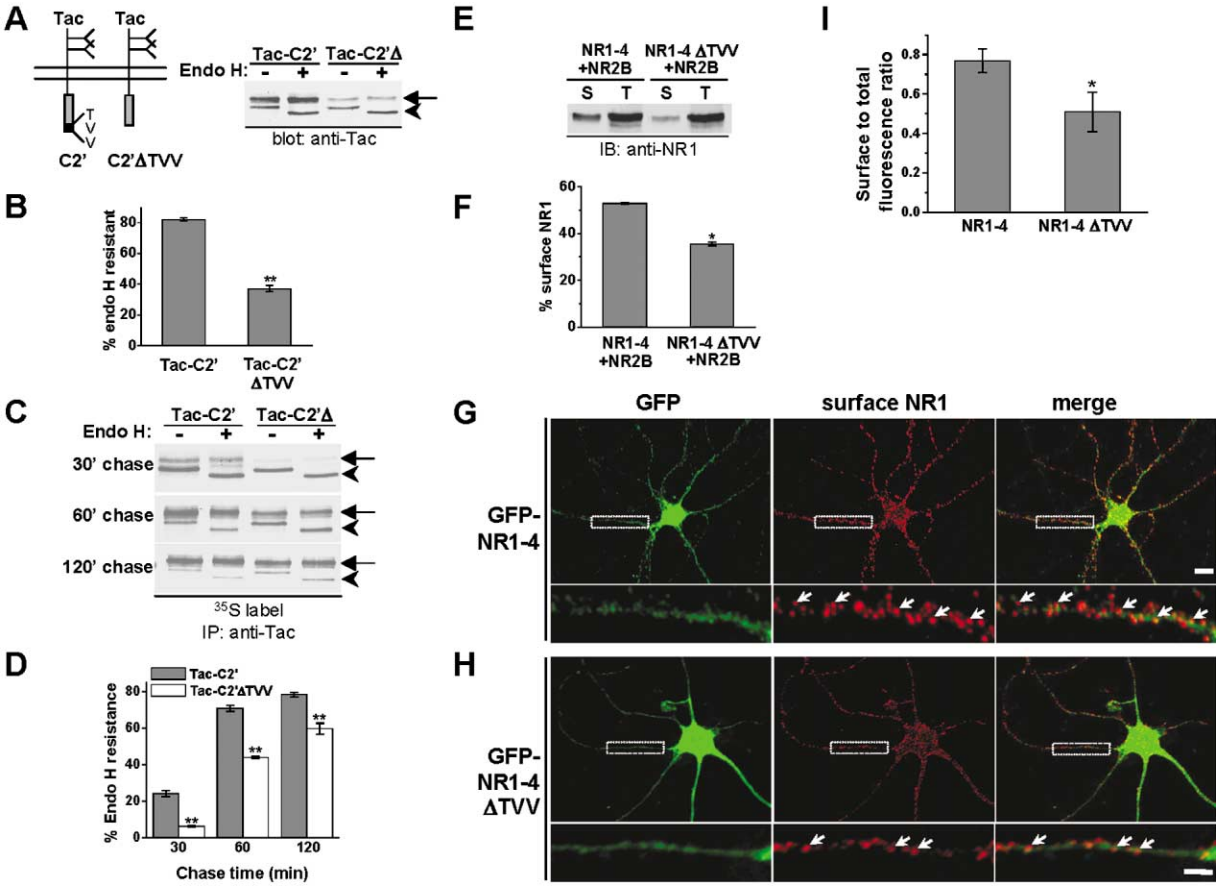

Figure 4. A Divaline-Based ER Export Motif in C2′ Facilitates NMDAR Surface Delivery

(A) Deletion of the TVV motif in C2′ (Tac-C2′Δ) decreased the steady-state levels of mature Tac fusion protein. Endo H sensitivity was measured by deglycosylation of COS7 cell lysates expressing Tac-C2′ or Tac-C2′ΔTVV prior to immunoblot analysis. Arrow and arrowhead as in Figure 3A.

(B) Means ± SEM of the percent mature Tac species from (A). n = 3, **p < 0.001 relative to Tac-C2′, t test.

(C) The TVV motif promotes ER export. ER-to-Golgi transport of newly synthesized Tac receptors was monitored by ^{35}S-pulse-chase followed by endo H deglycosylation of labeled Tac immunoprecipitates and autoradiography. Arrow and arrowhead as in (A).

(D) Increased rate of ER-to-Golgi transport in receptors containing the TVV motif. Plotted data represent means ± SEM of the percent endo H-resistant Tac receptor at various times of chase (n = 3). **p < 0.001 relative to Tac-C2′, t test.

(E) The TVV ER export signal increases surface expression of full-length NMDARs. COS7 cells expressing NR1-4/NR2B or NR1-4ΔTVV/NR2B heteromeric NMDARs were surface biotinylated, and surface membrane proteins (S) were isolated by neutravidin pull-down. Both surface membrane fractions (S) and total cell homogenates (T) were immunoblotted with anti-NR1 antibody.

(F) The ratio of surface/total NR1 from biotinylation experiments in (E) was quantified by phosphorimager analysis. Data represent means ± SEM. n = 3, *p < 0.05 relative to full-length NR1-4, t test.

(G and H) The TVV ER export signal increases synaptic delivery of NMDARs in hippocampal neurons. Hippocampal neurons (DIV 14) expressing GFP-NR1-4 (G) or GFP-NR1-4ΔTVV (H) were surface labeled with anti-GFP antibody prior to fixing and staining with fluorophore-conjugated secondary antibody. Total GFP-NR1-4 was visualized by endogenous GFP fluorescence. Arrows indicate surface NR1 puncta. Boxed regions in upper panels are magnified in lower panels. Scale bars equal 5 μm (upper panels) and 2 μm (lower panels).

(I) Quantification of GFP-NR1 surface expression in hippocampal neurons from (G) and (H). Data represent means ± SEM of surface NR1/total NR1 fluorescence ratios. n = 7–8, *p < 0.05 relative to full-length NR1-4, t test.

tained in the ER. Upon shift to the permissive temperature (32°C or lower), VSVG-YFP correctly folds, exits the ER, and traffics to the Golgi en route to the plasma membrane (Lippincott-Schwartz et al., 2000). This forward traffic can be arrested at the stage of ER exit by switching from 39.5°C to 10°C, allowing functional visualization of ER exit sites (Mezzacasa and Helenius, 2002). Using this approach, we found that after 10°C block, Tac receptors were abundant in the lacy ER membranes and showed modest accumulation at ER exit sites (Figure 5A, upper panels). Likewise, Tac-C2 receptors were present in the ER after 10°C block with very little detectable localization to ER exit sites (Figure 5A, middle panels). In contrast, appending the C2′ domain to Tac caused a marked accumulation of receptors at ER exit sites indicated by punctate VSVG-YFP labeling at 10°C (Figure 5A, lower panels), consistent with the more rapid export of Tac-C2′ receptors (Figure 4).

To investigate the mechanism underlying C2′-dependent recruitment to ER exit sites, we immobilized C2′ peptides on Sepharose 4B beads and tested whether the C2′ ER export signal binds COPII. As shown in Figure 5B, the C2′ peptide specifically pulled down the cargo binding Sec23/24 bimolecular complex of COPII from

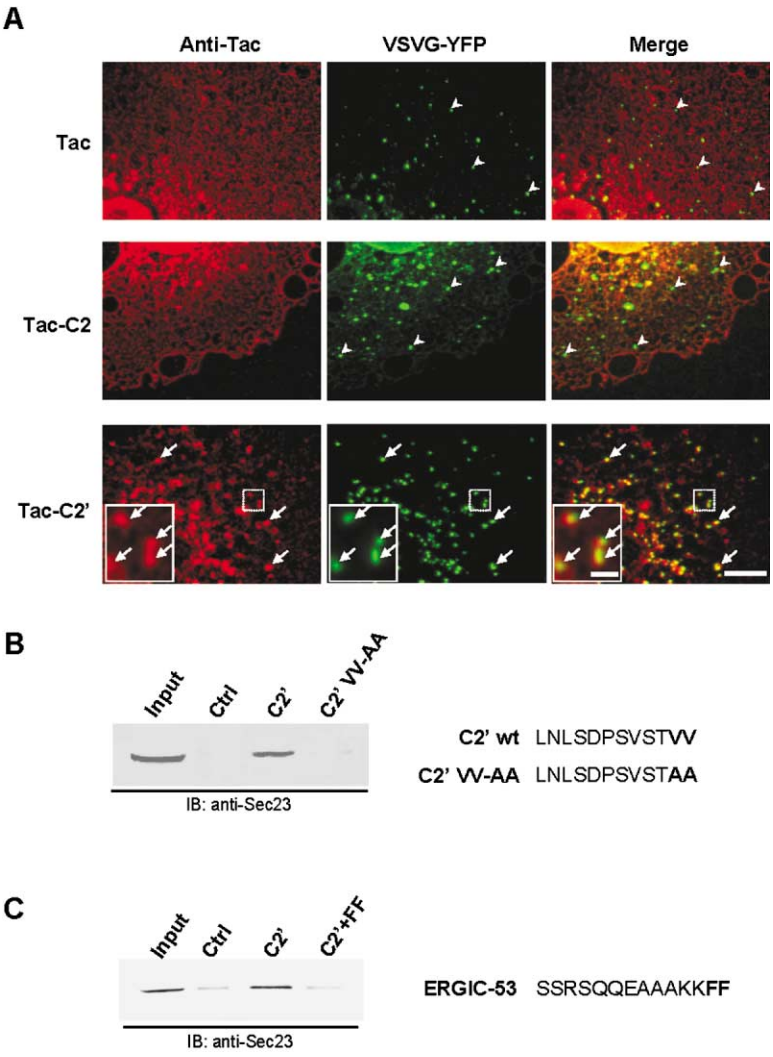

Figure 5. C2′ Recruits Receptors to ER Exit Sites by Binding COPII

(A) COS-7 cells expressing Tac, Tac-C2, or Tac-C2′ along with VSVG-YFP were incubated at 39.5°C for 18 hr and then switched to 10°C for 5 hr to allow protein accumulation at ER exits sites prior to fixing and staining for Tac (left). Punctate accumulations of VSVG-YFP (arrowheads and arrows) indicate ER exit sites. Arrows indicate colocalization of Tac-C2′ with VSVG-YFP. Insets are the higher power images of the boxed region showing the accumulations of Tac-C2′ at VSVG-YFP labeled ER exit sites. Scale bars equal 5 μm (large panels) and 1 μm (insets).

(B) The divaline motif of C2′ binds the Sec23/Sec24 complex of COPII coats. Pull-downs were performed on COS-7 cell lysates (input) using unconjugated control beads (Ctrl), C2′ peptide affinity resin (C2′), or VV-AA mutant C2′ peptide affinity resin (C2′ VV-AA), followed by immunoblot detection with anti-Sec23 antibody. Peptide sequences are shown on the right.

(C) Direct binding of C2′ to COPII coats. COPII pull-down assays were performed as in (B) in the absence (C2′) or presence (C2′+FF) of 2.5 mM ERGIC-53 C-terminal peptide (FF, sequence is shown on the right) to compete for binding to Sec23/24. Immunoblot analysis with an anti-Sec23 antibody was used to detect the Sec23/24 complex of COPII coats (left). The competing ERGIC-53 C-terminal peptide disrupts the COPII-C2′ binding interaction.

cell lysates. Substitution of alanines for the terminal valines completely abolished COPII binding. To confirm a direct interaction between C2′ and COPII, a peptide representing the C-terminal sequence of ERGIC-53 (Figure 5C) was included in the pull-down assay. This peptide contains a diphenylalanine motif that is known to bind to cargo recognition sites on the Sec24 subunit of Sec23/24 (Kappeler et al., 1997; Miller et al., 2003). Inclusion of excess ERGIC-53 peptide in the pull-down assay prevented the interaction between the immobilized C2′ peptide and Sec23/24 (Figure 5C), supporting competition for the same binding site. From these results, we conclude that the divaline ER export signal recruits receptors to ER exit sites by directly binding COPII.

Interaction with COPII Mediates the Accelerated Trafficking of C2′

In pulse-chase experiments, accelerated forward trafficking of Tac-C2′ depended on the C-terminal TVV motif of C2′ (Figures 4C and 4D). Our findings indicate that the terminal divaline motif of C2′ directly binds components of the COPII coat (Figure 5), providing a possible mechanism for this accelerated trafficking. However, the C-terminal TVV of C2′ has also been found to bind PDZ-domain-containing proteins (Standley et al., 2000). In order to determine which interaction—COPII or PDZ—was responsible for the accelerated forward trafficking of C2′-containing proteins, we expressed various mutants of the C2′ C terminus and determined the steady-state maturation of Tac-C2′ fusion proteins using endo H sensitivity assay (Figures 6A and 6B). Substitution of the −2 threonine with arginine (RVV), a mutation predicted to disrupt type I PDZ interactions while leaving the COPII interaction intact (Morais Cabral et al., 1996; Songyang et al., 1997; Nufer et al., 2002), had no effect on endo H sensitivity (82% ± 1% endo H-resistant, Tac-C2′; 85% ± 2.2%, Tac-C2′ RVV; Figures 6A and 6B). However, substitution of alanines for the terminal divaline motif (TAA), a mutation predicted to disrupt both PDZ interactions and COPII interactions (Figure 5), decreased the steady-state endo H-resistant pool of Tac-C2′ to 55% ± 2% (Figures 6A and 6B), a value identical to Tac alone (compare to Figure 3B). To reduce COPII binding without affecting PDZ interactions, we substituted arginine for the −1 valine (TRV). This mutation

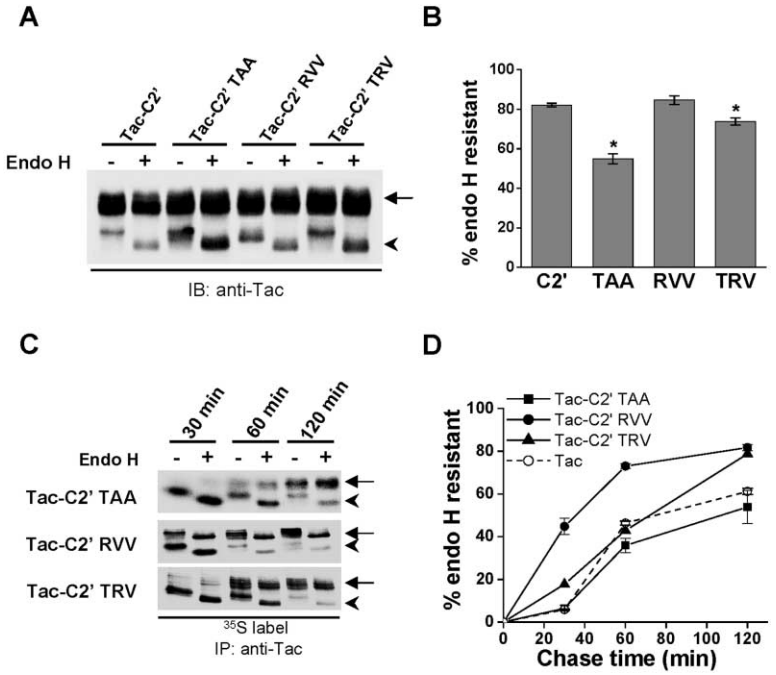

Figure 6. The ER Export Function of C2′ Is through COPII Binding and not PDZ Interactions

(A and B) Disruption of PDZ binding has no effect on the steady-state levels of mature Tac-C2′. (A) The endo H sensitivity of Tac-C2′, Tac-C2′ TAA, Tac-C2′ RVV, or Tac-C2′ TRV was measured as in Figure 3A. Arrow and arrowhead as in Figure 3A. (B) Quantification of the percent endo H-resistant Tac species from (A). n = 3, *p < 0.01 relative to Tac-C2′, t test.

(C and D) Disruption of the PDZ binding motif did not change the kinetics of ER-Golgi trafficking of Tac-C2′. (C) ER-to-Golgi transport of newly synthesized Tac-C2′ TAA, Tac-C2′ RVV, or Tac-C2′ TRV receptors was monitored by ^{35}S-pulse-chase as in Figure 3C. Arrow and arrowhead as in (A). (D) Plotted data represent means ± SEM of the percent endo H-resistant Tac receptor from (C) at various times of chase (n = 3).

partially disrupted the divaline motif and correspondingly caused a partial decrease in the mature pool of Tac-C2′ (Figure 6B).

To measure the effect of selectively disrupting PDZ versus COPII interactions on forward trafficking rates, we performed pulse-chase experiments. Monitoring endo H resistance using ^{35}S-pulse-chase analysis revealed that the RVV mutation (and presumed disruption of PDZ interactions) did not slow forward trafficking of Tac-C2′ (Figures 6C and 6D, compare with Figure 3D). However, the VV to AA substitution slowed the forward trafficking kinetics of Tac-C2′ to a rate similar to Tac alone. Substitution of only the penultimate valine with arginine (TRV) had an intermediate effect on trafficking kinetics, as expected from the steady-state results (Figures 6A and 6B). Together, these experiments show that the terminal valine in C2′ is critical for accelerated forward transport. The sufficiency of the divaline motif to facilitate forward transport in the absence of an intact PDZ binding motif strongly supports our model that COPII interactions, rather than PDZ interactions, mediate the accelerated forward trafficking of C2′-containing NMDARs.

Activity Bidirectionally Regulates the Surface Delivery Rate of NMDARs

The number of synaptic NMDARs is reciprocally regulated by neuronal activity (Rao and Craig, 1997; Liao et al., 1999; Watt et al., 2000; Crump et al., 2001). Our findings that activity regulates NR1 mRNA splicing at exon 22 (Figures 1 and 2) and thereby controls the inclusion or exclusion of an ER export motif in C2′ (Figures 3–6) suggest that activity may regulate accumulation of NMDARs at synapses by regulating trafficking at the level of the ER. To test this hypothesis, we measured the effect of activity on the rate at which newly synthesized NMDARs reached the cell surface. Cortical neurons treated for 48 hr with control solution, TTX (2 μM), or bicuculline (40 μM) were ^{35}S-labeled, and the cell surface appearance of NMDARs over time was measured using surface biotinylation followed by sequential neutravidin/anti-NR1 precipitation. Under control conditions, 19.9% ± 1.6% of newly synthesized NMDARs reached the cell surface within 12 hr (Figures 7A and 7B). This basal rate of surface delivery was markedly increased by activity blockade (TTX, 30.1% ± 1.4% after 12 hr; Figures 7A and 7B), consistent with the fact that these neurons preferentially express C2′-containing NR1 subunits (Figures 1 and 2). In contrast, cortical neurons experiencing elevated activity showed a substantial reduction in NMDAR surface delivery rate (Bicuc, 14.1% ± 0.3% after 12 hr; Figures 7A and 7B), consistent with exclusion of the C2′ ER export motif.

To further establish the bidirectional effect of activity on the forward trafficking of NMDARs, we used whole-cell recordings to measure the kinetics of NMDAR surface delivery in hippocampal neurons. We took advantage of the irreversible open channel blocker MK-801 and measured the recovery of NMDAR-mediated currents after complete MK-801 block. Under these conditions, current recovery reflects the delivery of new intracellular NMDARs to the cell surface (Lan et al., 2001). Basal whole-cell NMDAR-mediated currents were evoked by NMDA application (Figure 7C, left), and surface NMDARs were then blocked by simultaneous application of NMDA and MK-801 (20 μM) (Figure 7C, second current trace). After MK-801 block, currents evoked by NMDA were recorded every 10 min in response to NMDA application (Figure 7C). In control neurons, the amplitude of NMDA-evoked currents progressively recovered following MK-801 block, reaching 4.9% ± 1.7% of the initial amplitude after 1 hr (n = 5, Figure 7D). In neurons treated for 48 hr with TTX or bicuculline, NMDAR currents also recovered, but the rate of recovery was altered according to activity level. In TTX-treated neurons, NMDAR current recovery was nearly twice as rapid, reaching

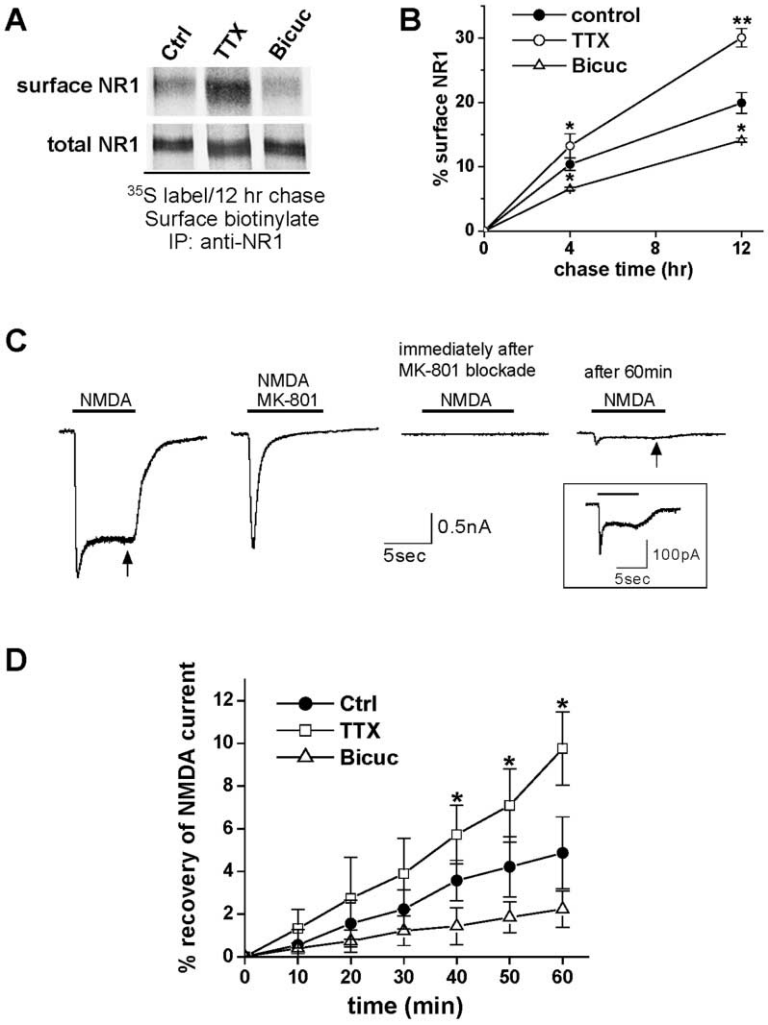

Figure 7. NMDAR Surface Delivery Rate Is Controlled by Activity Level

(A) Pulse-chase biotinylation assays of NMDAR surface delivery were performed on control, TTX-, and bicuculline-treated cortical neurons (see Experimental Procedures). The amount of ^{35}S-labeled NR1 appearing at the cell surface (surface NR1) after various times of chase provides a measure of forward trafficking rate.

(B) Quantitative analysis of NMDAR surface delivery. The percent of ^{35}S-labeled NR1 subunits at the cell surface measured by phosphorimager analysis was plotted as a function of time (means ± SEM, n = 3, *$p < 0.05$, **$p < 0.01$ relative to control at the same time point, t test).

(C) Measurement of NMDAR insertion by recovery from MK-801 block. A representative sequence of whole-cell currents evoked by NMDA application (500 μM) is shown. Recordings were made from hippocampal neurons (DIV 9–22) voltage-clamped at −40 mV. After complete block by MK-801 (20 μM; second current trace), NMDA currents gradually recovered over 60 min, indicating the appearance of new NMDARs (rightmost current trace). Arrows indicate steady-state NMDA-evoked currents. Inset at right shows the recovered NMDA-evoked current at an expanded scale.

(D) Kinetics of NMDAR surface delivery measured by recovery from MK-801 block. Data represent means ± SEM of the steady-state NMDA-evoked currents at various times after MK-801 block normalized to the initial currents before MK-801 application. n = 5, *$p < 0.05$ relative to control values at the same time point, t test.

9.8% ± 1.7% (n = 5) of basal currents after 60 min (Figure 7D). In contrast, bicuculline-treated neurons showed significantly slower recovery from MK-801 blockade (2.4% ± 1.1% after 60 min, n = 5; Figure 7D). These results indicate altered forward trafficking of NMDARs in response to activity and are remarkably consistent with the biochemical experiments above (Figures 7A and 7B). Together, these data provide strong evidence that chronic changes in neuronal activity regulate both forward trafficking and membrane delivery of NMDARs.

The NR1 C2′ Domain Is Required for Blockade-Induced Synaptic Targeting

To test whether the synaptic accumulation of NMDARs upon activity blockade is due to C2′-dependent forward trafficking, we expressed a GFP-tagged soluble C2′ peptide to disrupt the interaction of NR1 with COPII coats. Hippocampal neurons expressing GFP-C2′ were grown in the presence of AP5 (100 μM, 7 days) to induce NMNDR clustering, and NMDAR clusters were visualized and quantified by anti-NR1 staining. As shown in Figure 8, expression of C2′ peptide caused a decrease in the fluorescence intensity of detectable NMDAR puncta (Figures 8A and 8B), as well as a dramatic reduction in the number of NMDAR puncta (27 ± 4 NR1 puncta per 100 μm dendrite) compared with sister cultures expressing GFP alone (65 ± 6 NR1 puncta per 100 μm dendrite; Figure 8C). NR1 puncta in GFP-C2′-expressing neurons remained localized to excitatory synapses as indicated by colocalization with the postsynaptic scaffold protein Shank (Figure 8A). Moreover, the effect of C2′ peptide was specific for NMDARs, as the number of puncta positive for Shank remained unchanged (84 ± 7 per 100 μm dendrite for GFP, 71 ± 7 for GFP-C2′, $p > 0.05$, t test; Figure 8C). Further, expression of C2′ peptides lacking the divaline motif (GFP-C2′ΔTVV) had no effect on NMDAR clustering (data not shown). In all cases, NR1 and Shank puncta colocalized with markers of presynaptic terminals (data not shown). Likewise, in a separate set of experiments, GFP-C2′ had no effect on the density of synapsin puncta (synapsin puncta per 100 μm dendrite: GFP, 51 ± 8; GFP-C2′, 44 ± 8, $p > 0.05$, t test), indicating no change in the number of synaptic contacts.

To further demonstrate that synaptic accumulation of NMDARs after activity blockade is due to C2′-dependent forward trafficking, we measured the recovery from

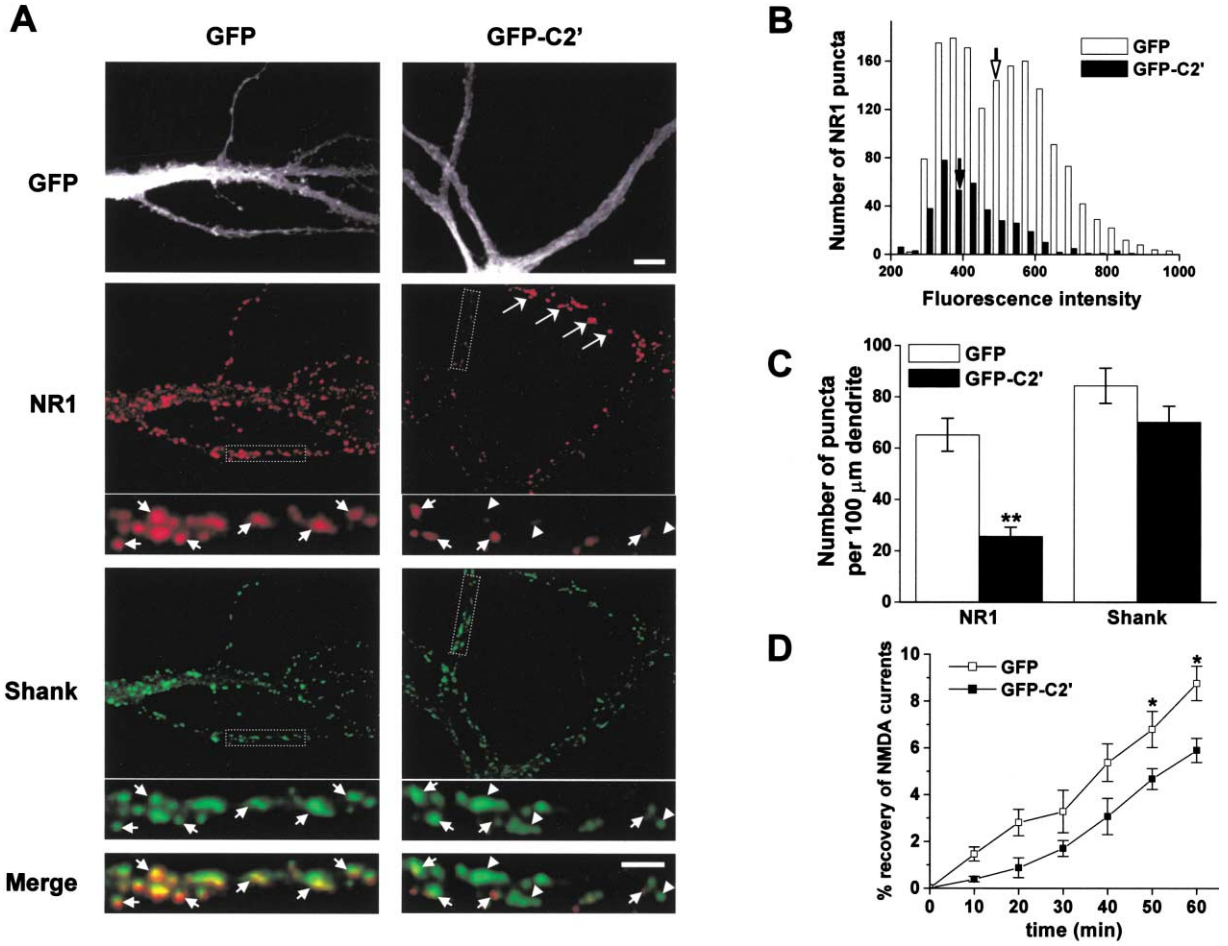

Figure 8. The NR1 C2′ Domain Is Required for Blockade-Induced Synaptic Accumulation of NMDARs.

(A) GFP or GFP-C2′ was expressed in hippocampal neurons (DIV 21) grown in the presence of 100 μM AP5 (7 days) to induce NMDAR clustering. NR1 (red) and Shank (green) clusters were visualized by immunofluorescent staining. Expression of GFP-C2′ caused a marked reduction in the number of detectable NR1 puncta but had no effect on Shank staining (right). Note that the GFP-C2′-transfected dendrite in the right panels displayed decreased NR1 clusters relative to the dendrite of a neighboring untransfected neuron in the same field (long arrows in NR1-stained panel). Short arrows indicate colocalized NR1/Shank clusters. Arrowheads indicate Shank puncta with no detectable NR1. Dashed white boxes indicate dendritic regions shown at higher power in accompanying panels. Scale bars equal 5 μm (upper panels) and 2 μm (higher power images).

(B) Histogram of the distribution of fluorescence intensity of NR1 puncta. Note that expression of GFP-C2′ decreases both the average intensity and the number of NMDAR clusters. Arrows indicate the median value of fluorescence intensity.

(C) Means ± SEM of the number of NR1 or Shank puncta per 100 μm dendrite from (A). n = 6–7 neurons from sister cultures for each condition, *$p < 0.05$ relative to the value from GFP-expressing neurons, t test.

(D) Expression of C2′ peptide decreases the insertion rate of NMDARs after activity blockade. Insertion rate of NMDARs in hippocampal neurons (DIV 9–22) expressing C2′ peptide after activity blockade (TTX, 1 μM, 2 days) was measured by recovery from MK-801 block as in Figure 7C. Data represent means ± SEM of the steady-state NMDA-evoked currents at various times after MK-801 block normalized to the initial currents before MK-801 application. n = 3–4, *$p < 0.05$ relative to the values from GFP-expressing neurons at the same time point, t test.

MK-801 block in neurons expressing GFP or GFP-C2′ as in Figure 7C. After chronic TTX treatment (1 μM, 48 hr), expression of GFP in neurons showed no effect on NMDAR insertion rate as compared with TTX-treated, nontransfected neurons, reaching 8.8% ± 1.5% (n = 4) of basal currents after 60 min (compare Figures 8D and 7D). In contrast, expression of soluble GFP-C2′ peptide significantly decreased the insertion rate of NMDARs with only 5.9% ± 0.9% recovery of basal currents after 60 min (n = 3, $p < 0.05$, t test; Figure 8D). Together, these data indicate that the C2′ domain of NR1 regulates the synaptic targeting of NMDARs following prolonged activity blockade, supporting a role for C2′-mediated ER export in NMDAR surface delivery. Finally, these results provide further evidence indicating that inclusion or exclusion of exon 22 in NR1 pre-mRNA is a key determinant of NMDAR forward trafficking and synaptic targeting during synaptic homeostasis.

Discussion

In the present study, we have demonstrated that activity regulates NMDAR synaptic targeting through an unexpected mechanism involving mRNA splicing and regu-

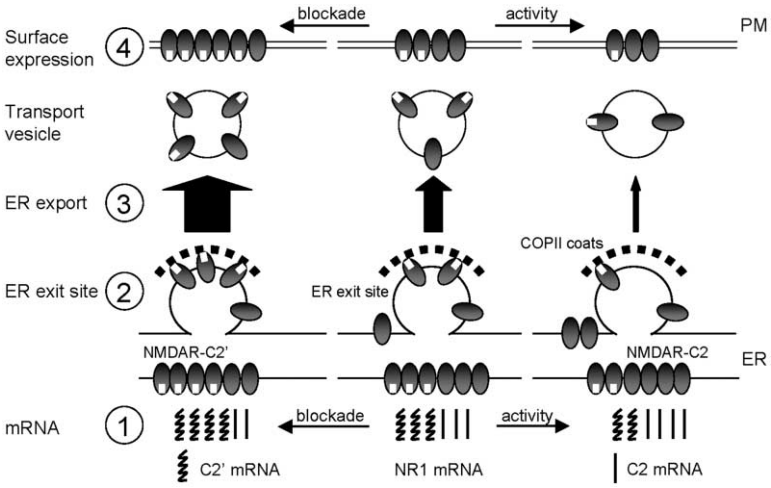

Figure 9. Proposed Model for Activity-Dependent Synaptic Targeting of NMDARs

In this simplified model, prolonged synaptic blockade results in (1) exclusion of exon 22 in NR1 mRNA leading to synthesis of NR1 subunits containing the C2′ domain. (2) The divaline ER export signal in C2′ interacts with COPII coats to recruit nascent receptors to ER exit sites. (3) Recruitment to ER exit sites facilitates ER export and thereby accelerates forward trafficking of NMDARs. (4) As a result, increased numbers of NMDARs are delivered to the synapse. In contrast, a precisely opposite sequence of events (inclusion of exon 22 and thus synthesis of NR1-C2, decreased ER export, decreased surface accumulation) occurs in response to increased neuronal activity.

lated ER export. In response to prolonged activity blockade, exon 22 is excluded from NR1 mRNA, resulting in the synthesis of NR1 subunits containing the alternate C2′ domain at the distal C terminus. The C2′ domain in turn contains a divaline-based ER export motif that enhances the export of newly synthesized NMDARs from the ER by directly binding COPII coats at ER exit sites. As ER export is rate limiting, more rapid export increases surface delivery and synaptic targeting of NMDARs (Figure 9).

NMDAR ER Export, Homeostasis, and Metaplasticity

Activity-dependent ER export of NMDARs may provide a cellular mechanism for synaptic homeostasis and may determine the propensity of synapses to undergo potentiation or depression—a process termed metaplasticity (Abraham and Bear, 1996). In response to altered activity over a period of days, excitatory synaptic strength at glutamatergic synapses is scaled in a compensatory manner, with mEPSC amplitudes increasing after prolonged blockade and decreasing after chronic synaptic activation (Turrigiano et al., 1998; Watt et al., 2000; Desai et al., 2002). This homeostatic plasticity occurs in neuronal culture models (O'Brien et al., 1998; Turrigiano et al., 1998; Lissin et al., 1999) and during critical periods in vivo (Desai et al., 2002) and is thought to provide a countervailing mechanism to rapid forms of Hebbian plasticity by ensuring that neurons remain in an optimal firing frequency range (Turrigiano and Nelson, 2000). Although the homeostatic changes in mEPSC amplitudes reflect synaptic AMPARs, NMDAR-mediated currents are scaled up or down by chronic changes in activity proportionally with AMPAR-mediated currents (Watt et al., 2000). Indeed, prolonged visual experience and deprivation alternately diminishes or enhances NMDAR-mediated transmission in visual cortical neurons (Philpot et al., 2001, 2003). This activity-dependent regulation of NMDAR-mediated currents is accompanied by corresponding physical accumulation or loss of NMDARs from the postsynaptic membrane (Rao and Craig, 1997; Liao et al., 1999; Crump et al., 2001; Ehlers, 2003). Here we have shown that the activity-dependent accumulation or reduction in synaptic NMDARs is a direct consequence of altered ER export. By regulating the kinetics of NMDAR forward trafficking and thus the number of synaptic NMDARs, the magnitude of NMDAR-mediated signals can be tuned to the level of activity. In addition to affecting basal transmission, control over the magnitude and duration of NMDAR-mediated signals is of fundamental importance for setting the synaptic modification threshold for subsequent activity-dependent plasticity (Abraham and Bear, 1996; Philpot et al., 2003). Surprisingly, the mechanism revealed here for NMDARs is quite distinct from that utilized by AMPARs, which accumulate at synapses upon prolonged activity blockade due to a decrease in their rate of turnover (O'Brien et al., 1998). Thus, although the number of AMPARs and NMDARs at the postsynaptic membrane scale in parallel (Watt et al., 2000), the scaling of these two classes of homologous glutamate receptors is alternately regulated at the level of protein degradation and ER export, respectively.

ER Export as an Activity-Regulated Checkpoint

Quality control in the ER is a key feature of ion channel biogenesis, proper stoichiometric assembly, and surface expression and has been proposed to control the overall number of channels at the cell surface (Ma et al., 2001; Ellgaard and Helenius, 2003). To date, ER retention and ER export have been considered intrinsic properties of channel assembly caused by masking of ER retention signals or exposure of ER export signals (Ma et al., 2001; Greger et al., 2002). The possibility that export from the ER can act as a regulated checkpoint sensitive to the signaling needs of the neuron or prior history of activity has been postulated (Scott et al., 2001) but has remained an open question. Here we have shown that activity level directly regulates ER export of nascent NMDARs. This switch in ER export rate provides a rheostat-like feedback mechanism for adjusting the pool of NMDARs available for surface expression or synaptic incorporation. Indeed, rapidly exported NMDARs containing NR1-C2′ exhibit higher basal surface expression (Okabe et al., 1999), and the presence of NR1-C2 versus NR1-C2′—slow and fast exported receptors, respectively—exerts a significant effect on NMDAR potentiation by

both PKC and tetanic stimulation (Lan et al., 2001; Grosshans et al., 2002). Thus, ER export may be the first of several NMDAR trafficking steps regulated by activity, in essence acting as a "master regulatory valve" for a pipeline of NMDARs supplied for later exocytotic events.

ER exit is mediated by COPII-coated vesicles that bud off from defined points on the ER membrane (Barlowe, 2002). The packaging and concentrating of cargo into budding COPII vesicles involves direct binding of export signals with the Sec24 subunit of the Sec23/24 complex (Kappeler et al., 1997; Barlowe, 2002; Miller et al., 2003; Mossessova et al., 2003). Results provided here demonstrate that the divaline motif of the NR1 C2′ domain likewise binds Sec23-Sec24, providing to our knowledge the first demonstration of a COPII binding ER export motif in an ion channel. Consistent with our findings, C-terminal valine residues facilitate ER export of type I integral membrane proteins (Nufer et al., 2002), suggesting that direct COPII association may be a conserved mechanism across broad families of integral membrane proteins.

Interestingly, the positional requirement of COPII binding valine motifs, namely at the very C terminus, is shared by type I PDZ binding motifs (T(S)XV), suggesting that such motifs have dual functions—an initial ER export function via COPII and a subsequent targeting function via a PDZ protein. For a number of plasma membrane proteins (Fernandez-Larrea et al., 1999; Standley et al., 2000), surface expression has been thought to rely upon PDZ interaction. However, it is likely that broad classes of type I PDZ binding motifs also interact with COPII. In light of our findings, conclusions regarding trafficking mechanisms previously ascribed to PDZ interactions may warrant reexamination. Indeed, recent reports have shown that terminal valine motifs in a variety of contexts can accelerate forward trafficking (Nufer et al., 2002). We propose that many, if not all, type I PDZ binding motifs in integral membrane proteins also bind COPII in early phases of secretory trafficking.

Activity-Dependent mRNA Splicing of NR1

Brain-specific alternative splicing generates much of the diversity needed in proteins involved in neurotransmission and nervous system development (Dredge et al., 2001; Grabowski and Black, 2001). Indeed, numerous developmental and region-specific changes in mRNA splicing have been documented throughout the nervous system under both physiological and pathological conditions (Dredge et al., 2001; Grabowski and Black, 2001), although the mechanisms regulating such splicing remain almost completely unknown.

Results presented here support a direct link between NR1 mRNA splicing, activity, and synaptic homeostasis. In particular, our findings suggest a signaling pathway whereby activation of NMDARs triggers a cascade that leads to inclusion of exon 22 in NR1 mRNA. In nonneuronal cells, extracellular stimuli and protein kinase activation alter the splicing of several transcripts (Grabowski and Black, 2001; Xie and Black, 2001) through poorly characterized cellular signaling pathways. In many cases, the change in splicing is independent of new protein synthesis, indicating that a kinase or other enzyme may directly modify the splicing apparatus. Indeed, substantial evidence implicates reversible protein phosphorylation in spliceosome assembly and disassembly as well as splicing catalysis (Dredge et al., 2001; Grabowski and Black, 2001). In this regard it is interesting to note that activity-dependent synaptic targeting of NMDARs is regulated by protein kinase pathways (Crump et al., 2001; Fong et al., 2002), raising the intriguing possibility that neuronal splicing factors acting on the NR1 pre-mRNA may be regulatory targets of these kinase cascades. Further, while the splicing of exon 22 is regulated by activity, levels of NMDAR protein containing exon 21 remain stable regardless of activity blockade (Rao and Craig, 1997). This high degree of specificity in the exons subject to regulated splicing suggests specific *cis*-acting elements within the exons themselves or neighboring intronic sequences. Clearly, it will be important for future studies to delineate the relevant signaling pathways, molecular targets, and RNA elements between altered neuronal activity and regulation of splicing at exon 22. More broadly, coordination of mRNA splicing may provide a general mechanism for activity-dependent modification of CNS synapses.

Experimental Procedures

Antibodies and DNA Constructs

Anti-Tac (Covance, 1:500), anti-GFP (Chemicon, 1:1000), anti-NR1 (S3C11, 1:250), and anti-Shank (a gift from Dr. Eunjoon Kim, 1:250) antibodies were used for immunofluorescence. For Western blots or immunoprecipitations, anti-Tac (Santa Cruz Biotechnology, 1:1000), anti-NR1(54.1, Pharmingen International, 1:1500), anti-C2′ (1233, 1:1000), anti-C2 (1683, 1:2000), or anti-Sec23 (a gift from Dr. Wanjin Hong, 1:2000) antibodies were used.

Generation of Tac-NR1 constructs was accomplished as previously described (Scott et al., 2001). For GFP-C2′ construct, a pair of primers (5′-GGTGTACAAGCAGTACCATCCCACTGATATCACG-3′ and 5′-ATTTGCGGCCGCTCAGCTGACCGAGGGATCTGAGAG-3′) were used to amplify the C2′ domain, which was then inserted into pEGFP-N1 (Clontech). VSVG-YFP was a generous gift from Dr. Kai Simons. GFP-NR1 was kindly provided by Dr. Stefano Vicini. GFP-NR1-4 ΔTVV was generated by inserting a stop codon before Thr904 (in NR1-4b) using Stratagene's Site-Directed Mutagenesis Kit following the manufacturer's instructions.

Cell Culture and Transfection

Hippocampal neurons, cortical neurons, and COS-7 cells were cultured and transfected as previously described (Ehlers, 2000; Scott et al., 2001).

Metabolic Labeling and Endo H Resistance Assay

COS-7 cells, transfected for 48 hr, were washed three times with Hank's balance salt solution and starved for 30 min at 37°C in DMEM/methionine/cysteine-free medium. Cells were then labeled with 500 μCi/ml ^{35}S-methionine/cysteine for 20 min and chased with conditioned media supplemented with 2 μM methionine for the times indicated. After chase, cells were washed with ice-cold PBS, lysed in lysis buffer (20 mM Tris 7.4, 150 mM NaCl, 1 mM EDTA, 1% Triton X-100, protease inhibitor cocktail), and immunoprecipitated with an anti-Tac antibody (2 μg/IP). The immunoprecipitate was eluted in 30 μl elution buffer (50 mM Tris 8.0, 1% SDS, 0.1% β-mercaptoethanol) by boiling for 5 min. The resulting elution was mixed with 30 μl of endo H digestion buffer (150 mM sodium citrate [pH 5.5], 2× PMSF) and then divided into two equal aliquots. 50 mU of endo H was added to one aliquot and incubated at 37°C for 5 hr. The reaction was stopped by adding an equal volume of 2× SDS-PAGE loading buffer.

Chymotrypsin Proteolysis

Cortical neurons (9–10 DIV) were metabolically labeled with 500 μCi/ml ^{35}S-cysteine/methionine and chased as described above. After chase, neurons were washed with Hank's balanced salt solution and treated with 1 mg/ml chymotrypsin for 10 min at 37°C. The intracellular protected NR1 subunits were then immunoprecipitated with anti-NR1 antibodies (1683 for C2-containing NR1, 1233 for C2′-containing NR1). The NR1 precipitate was separated on SDS-PAGE, scanned on a phosphorimager (Molecular Dynamics), and quantified using ImageQuant software (Molecular Dynamics). The trafficking rate of NR1 was expressed as the ratio of intracellular C2′ ($C2'_{int}$) versus intracellular NR1 ($C2_{int} + C2'_{int}$).

Immunofluorescence

Neurons were fixed and permeabilized sequentially with 4% paraformaldehyde plus 4% sucrose (10 min at 4°C), −20°C methanol (10 min at 4°C), and 0.2% Triton X-100 in PBS (10 min at 4°C). Neurons were then blocked with 10% goat serum in PBS for 1 hr at 37°C and incubated with primary antibodies at 4°C overnight and with secondary antibodies at RT for 1 hr. For surface labeling, primary antibodies were applied on live neurons at 4°C for 30 min before fixation.

Quantitative immunofluorescence was performed using a Yokogawa spinning disk confocal (Solamere Technology Group) and analyzed using Metamorph (Universal Imaging Corporation). The maximum projection images were thresholded to define puncta. Clusters whose intensity were 2-fold or more above the fluorescence background were considered as puncta.

Surface Biotinylation

Cortical neurons (DIV 10–12) were metabolically labeled and chased as described above, washed with ice-cold PBS, and surface biotinylated as previously described (Ehlers, 2000). Total NR1 was then immunoprecipitated using an anti-NR1 antibody (54.1). Following elution from protein A/G beads, surface NR1 was isolated by immunoprecipitation of biotin-linked NR1 with NeutrAvidin beads (Pierce).

RNase Protection Assay

Two primer sets were used to amplify probes for total NR1 (5′-CGG GATCCGTACCATGTACCGGCACATGG-3′, 5′-GGGGTACCGTTGC AGGAGCATTGCTGCGG-3′) and C2′-containing NR1 (5′-CGGGATC CTAGGGAGAGCTGAGACGCCC-3′, 5′-GGGGTACCGCCCAGGGTGG GCAGTCTCT-3′). The resulting PCR products were cloned into pSPT19 plasmid (Roche). Total RNAs from cortical neurons were isolated using Trizol reagent from Invitrogen. 40 μg total RNA was used in each RPA assay. Probes were labeled with ^{32}P-CTP using SP6/T7 RNA polymerases (Roche). RPA assays were performed using RPAIII TM Ribonuclease Protection Assay Kit (Ambion) according to manufacturer's instruction. Protected probes were separated on 6% gel, scanned on a phosphorimager, and quantified using ImageQuant 5.0 software. Data is expressed as C2′ NR1/total NR1 ratio related to control.

Electrophysiology

Whole-cell voltage clamp recordings were performed on cortical neurons (DIV 9–22). Neurons cultured at a high density on a glass coverslip were transferred to a recording chamber mounted on the stage of an inverted microscope (Nikon, Tokyo). The recording chamber was continuously perfused with extracellular solution containing (in mM): 150 NaCl, 5 KCl, 2 $CaCl_2$, 10 HEPES, 30 glucose, 0.02 glycine, 0.001 TTX, and 0.01 bicuculline methiodide with no added magnesium (330 ± 5 mOsm/l [pH 7.4]). Electrodes were pulled from glass capillary tubes (Narishige, Tokyo) and fire-polished. The recording pipettes were filled with a solution containing (in mM): 70 K_2SO_4, 2.5 $MgCl_2$, 1 EGTA, 0.1 $CaCl_2$, 25 HEPES, 60 N-methyl-D-glucamine, 2 Na_2ATP, 0.2 Na_2GTP, and 0.1 leupeptin (300 ± 5 mOsm/l [pH 7.2]). The resistance of the filled pipettes ranged from 3 to 5 MΩ. In bicuculline or TTX treatment, 20 μM bicuculline or 1 μM TTX was added to culture medium for 2 to 3 days before recordings. In C2′ peptide experiments, neurons were transfected with GFP or GFP-C2′ one day after adding TTX and allowed to express C2′ peptide for another 2 days in the presence of TTX before recordings. Recordings were obtained with a MultiClamp 700A amplifier (Axon Instruments, Foster City, CA) controlled with a Pentium PC running MultiClamp Commander 1.1 and pClamp 8.02 (Axon Instruments). Signals were filtered at 4 kHz and sampled at 10 kHz. If the series resistance changed from initial value during recording, the recording was terminated or the data were discarded.

Acknowledgments

We thank Chi Zhang and Haiwei Zhang for excellent technical support, Stefano Vicini for providing the GFP-NR1 construct, Eunjoon Kim for anti-Shank antibody, Wanjin Hong for anti-Sec23 antibody, and Peter Reinhart for use of equipment. We also thank George Augustine, Thomas Blanpied, Guoping Feng, Juliet Hernandez, Larry Katz, Rich Mooney, Isabel Perez-Otano, and Pate Skene for helpful comments on the manuscript. This work was supported by grants to D.B.S. from the NIAAA (F31 AA 13220) and to M.D.E. from the NIH (NS39402), the American Heart Association, and a Broad Scholar Award.

Received: May 27, 2003
Revised: September 30, 2003
Accepted: October 7, 2003
Published: October 29, 2003

References

Abraham, W.C., and Bear, M.F. (1996). Metaplasticity: the plasticity of synaptic plasticity. Trends Neurosci. *19*, 126–130.

Barlowe, C. (2002). COPII-dependent transport from the endoplasmic reticulum. Curr. Opin. Cell Biol. *14*, 417–422.

Barria, A., and Malinow, R. (2002). Subunit-specific NMDA receptor trafficking to synapses. Neuron *35*, 345–353.

Carroll, R.C., and Zukin, R.S. (2002). NMDA-receptor trafficking and targeting: implications for synaptic transmission and plasticity. Trends Neurosci. *25*, 571–577.

Crump, F.T., Dillman, K.S., and Craig, A.M. (2001). cAMP-dependent protein kinase mediates activity-regulated synaptic targeting of NMDA receptors. J. Neurosci. *21*, 5079–5088.

Cull-Candy, S., Brickley, S., and Farrant, M. (2001). NMDA receptor subunits: diversity, development and disease. Curr. Opin. Neurobiol. *11*, 327–335.

Desai, N.S., Cudmore, R.H., Nelson, S.B., and Turrigiano, G.G. (2002). Critical periods for experience-dependent synaptic scaling in visual cortex. Nat. Neurosci. *5*, 783–789.

Dredge, B.K., Polydorides, A.D., and Darnell, R.B. (2001). The splice of life: alternative splicing and neurological disease. Nat. Rev. Neurosci. *2*, 43–50.

Ehlers, M.D. (2000). Reinsertion or degradation of AMPA receptors determined by activity-dependent endocytic sorting. Neuron *28*, 511–525.

Ehlers, M.D. (2003). Activity level controls postsynaptic composition and signaling via the ubiquitin-proteasome system. Nat. Neurosci. *6*, 231–242.

Ehlers, M.D., Tingley, W.G., and Huganir, R.L. (1995). Regulated subcellular distribution of the NR1 subunit of the NMDA receptor. Science *269*, 1734–1737.

Ehlers, M.D., Zhang, S., Bernhadt, J.P., and Huganir, R.L. (1996). Inactivation of NMDA receptors by direct interaction of calmodulin with the NR1 subunit. Cell *84*, 745–755.

Ehlers, M.D., Fung, E.T., O'Brien, R.J., and Huganir, R.L. (1998). Splice variant-specific interaction of the NMDA receptor subunit NR1 with neuronal intermediate filaments. J. Neurosci. *18*, 720–730.

Ellgaard, L., and Helenius, A. (2003). Quality control in the endoplasmic reticulum. Nat. Rev. Mol. Cell Biol. *4*, 181–191.

Fernandez-Larrea, J., Merlos-Suarez, A., Urena, J.M., Baselga, J., and Arribas, J. (1999). A role for a PDZ protein in the early secretory pathway for the targeting of proTGF-alpha to the cell surface. Mol. Cell *3*, 423–433.

Fong, D.K., Rao, A., Crump, F.T., and Craig, A.M. (2002). Rapid synaptic remodeling by protein kinase C: reciprocal translocation

of NMDA receptors and calcium/calmodulin-dependent kinase II. J. Neurosci. *22*, 2153–2164.

Grabowski, P.J., and Black, D.L. (2001). Alternative RNA splicing in the nervous system. Prog. Neurobiol. *65*, 289–308.

Greger, I.H., Khatri, L., and Ziff, E.B. (2002). RNA editing at arg607 controls AMPA receptor exit from the endoplasmic reticulum. Neuron *34*, 759–772.

Grosshans, D.R., Clayton, D.A., Coultrap, S.J., and Browning, M.D. (2002). LTP leads to rapid surface expression of NMDA but not AMPA receptors in adult rat CA1. Nat. Neurosci. *5*, 27–33.

Heynen, A.J., Quinlan, E.M., Bae, D.C., and Bear, M.F. (2000). Bidirectional, activity-dependent regulation of glutamate receptors in the adult hippocampus in vivo. Neuron *28*, 527–536.

Huh, K.H., and Wenthold, R.J. (1999). Turnover analysis of glutamate receptors identifies a rapidly degraded pool of the N-methyl-D-aspartate receptor subunit, NR1, in cultured cerebellar granule cells. J. Biol. Chem. *274*, 151–157.

Kappeler, F., Klopfenstein, D.R., Foguet, M., Paccaud, J.P., and Hauri, H.P. (1997). The recycling of ERGIC-53 in the early secretory pathway. ERGIC-53 carries a cytosolic endoplasmic reticulum-exit determinant interacting with COPII. J. Biol. Chem. *272*, 31801–31808.

Lan, J.Y., Skeberdis, V.A., Jover, T., Grooms, S.Y., Lin, Y., Araneda, R.C., Zheng, X., Bennett, M.V., and Zukin, R.S. (2001). Protein kinase C modulates NMDA receptor trafficking and gating. Nat. Neurosci. *4*, 382–390.

Liao, D., Zhang, X., O'Brien, R., Ehlers, M.D., and Huganir, R.L. (1999). Regulation of morphological postsynaptic silent synapses in developing hippocampal neurons. Nat. Neurosci. *2*, 37–43.

Lippincott-Schwartz, J., Roberts, T.H., and Hirschberg, K. (2000). Secretory protein trafficking and organelle dynamics in living cells. Annu. Rev. Cell Dev. Biol. *16*, 557–589.

Lissin, D.V., Carroll, R.C., Nicoll, R.A., Malenka, R.C., and von Zastrow, M. (1999). Rapid, activation-induced redistribution of ionotropic glutamate receptors in cultured hippocampal neurons. J. Neurosci. *19*, 1263–1272.

Lodish, H.F. (1988). Transport of secretory and membrane glycoproteins from the rough endoplasmic reticulum to the Golgi. A rate-limiting step in protein maturation and secretion. J. Biol. Chem. *263*, 2107–2110.

Ma, D., Zerangue, N., Lin, Y.F., Collins, A., Yu, M., Jan, Y.N., and Jan, L.Y. (2001). Role of ER export signals in controlling surface potassium channel numbers. Science *291*, 316–319.

Malinow, R., and Malenka, R.C. (2002). AMPA receptor trafficking and synaptic plasticity. Annu. Rev. Neurosci. *25*, 103–126.

Mezzacasa, A., and Helenius, A. (2002). The transitional ER defines a boundary for quality control in the secretion of tsO45 VSV glycoprotein. Traffic *3*, 833–849.

Miller, E.A., Beilharz, T.H., Malkus, P.N., Lee, M.C., Hamamoto, S., Orci, L., and Schekman, R. (2003). Multiple cargo binding sites on the COPII subunit Sec24p ensure capture of diverse membrane proteins into transport vesicles. Cell *114*, 497–509.

Morais Cabral, J.H., Petosa, C., Sutcliffe, M.J., Raza, S., Byron, O., Poy, F., Marfatia, S.M., Chishti, A.H., and Liddington, R.C. (1996). Crystal structure of a PDZ domain. Nature *382*, 649–652.

Mossessova, E., Bickford, L.C., and Goldberg, J. (2003). SNARE selectivity of the COPII coat. Cell *114*, 483–495.

Nufer, O., Guldbrandsen, S., Degen, M., Kappeler, F., Paccaud, J.P., Tani, K., and Hauri, H.P. (2002). Role of cytoplasmic C-terminal amino acids of membrane proteins in ER export. J. Cell Sci. *115*, 619–628.

O'Brien, R.J., Kamboj, S., Ehlers, M.D., Rosen, K.R., Fischbach, G.D., and Huganir, R.L. (1998). Activity-dependent modulation of synaptic AMPA receptor accumulation. Neuron *21*, 1067–1078.

Okabe, S., Miwa, A., and Okado, H. (1999). Alternative splicing of the C-terminal domain regulates cell surface expression of the NMDA receptor NR1 subunit. J. Neurosci. *19*, 7781–7792.

Philpot, B.D., Sekhar, A.K., Shouval, H.Z., and Bear, M.F. (2001). Visual experience and deprivation bidirectionally modify the composition and function of NMDA receptors in visual cortex. Neuron *29*, 157–169.

Philpot, B.D., Espinosa, J.S., and Bear, M.F. (2003). Evidence for altered NMDA receptor function as a basis for metaplasticity in visual cortex. J. Neurosci. *23*, 5583–5588.

Quinlan, E.M., Philpot, B.D., Huganir, R.L., and Bear, M.F. (1999). Rapid, experience-dependent expression of synaptic NMDA receptors in visual cortex in vivo. Nat. Neurosci. *2*, 352–357.

Rao, A., and Craig, A.M. (1997). Activity regulates the synaptic localization of the NMDA receptor in hippocampal neurons. Neuron *19*, 801–812.

Roche, K.W., Standley, S., McCallum, J., Dune Ly, C., Ehlers, M.D., and Wenthold, R.J. (2001). Molecular determinants of NMDA receptor internalization. Nat. Neurosci. *4*, 794–802.

Scott, D.B., Blanpied, T.A., Swanson, G.T., Zhang, C., and Ehlers, M.D. (2001). An NMDA receptor ER retention signal regulated by phosphorylation and alternative splicing. J. Neurosci. *21*, 3063–3072.

Songyang, Z., Fanning, A.S., Fu, C., Xu, J., Marfatia, S.M., Chishti, A.H., Crompton, A., Chan, A.C., Anderson, J.M., and Cantley, L.C. (1997). Recognition of unique carboxyl-terminal motifs by distinct PDZ domains. Science *275*, 73–77.

Standley, S., Roche, K.W., McCallum, J., Sans, N., and Wenthold, R.J. (2000). PDZ domain suppression of an ER retention signal in NMDA receptor NR1 splice variants. Neuron *28*, 887–898.

Turrigiano, G.G., and Nelson, S.B. (2000). Hebb and homeostasis in neuronal plasticity. Curr. Opin. Neurobiol. *10*, 358–364.

Turrigiano, G.G., Leslie, K.R., Desai, N.S., Rutherford, L.C., and Nelson, S.B. (1998). Activity-dependent scaling of quantal amplitude in neocortical neurons. Nature *391*, 892–896.

Watt, A.J., van Rossum, M.C., MacLeod, K.M., Nelson, S.B., and Turrigiano, G.G. (2000). Activity coregulates quantal AMPA and NMDA currents at neocortical synapses. Neuron *26*, 659–670.

Wenthold, R.J., Prybylowski, K., Standley, S., Sans, N., and Petralia, R.S. (2003). Trafficking of NMDA receptors. Annu. Rev. Pharmacol. Toxicol. *43*, 335–358.

Xia, H., Hornby, Z.D., and Malenka, R.C. (2001). An ER retention signal explains differences in surface expression of NMDA and AMPA receptor subunits. Neuropharmacology *41*, 714–723.

Xie, J., and Black, D.L. (2001). A CaMK IV responsive RNA element mediates depolarization-induced alternative splicing of ion channels. Nature *410*, 936–939.

Zukin, R.S., and Bennett, M.V. (1995). Alternatively spliced isoforms of the NMDARI receptor subunit. Trends Neurosci. *18*, 306–313.